Original article

Nuclear Medicine Communications

Measurement of ^{18}F-FDG PET tumor heterogeneity improves early assessment of response to bevacizumab compared with the standard size and uptake metrics in a colorectal cancer model

Usman Bashir[a,*], Amanda Weeks[b,*], Jayant S. Goda[b], Muhammad Siddique[b], Vicky Goh[a,d] and Gary J. Cook[a,c]

Purpose **Treatment of metastatic colorectal cancer frequently includes antiangiogenic agents such as bevacizumab. Size measurements are inadequate to assess treatment response to these agents, and newer response assessment criteria are needed. We aimed to evaluate ^{18}F-FDG PET-derived texture parameters in a preclinical colorectal cancer model as alternative metrics of response to treatment with bevacizumab.**

Materials and methods **Fourteen CD1 athymic mice injected in the flank with 5×106 LS174T cells (human colorectal carcinoma) were either untreated controls ($n = 7$) or bevacizumab treated ($n = 7$). After 2 weeks, mice underwent ^{18}F-FDG PET/CT. Calliper-measured tumor growth (Δ_{vol}) and final tumor volume (Vol_{cal}), ^{18}F-FDG PET metabolically active volume (Vol_{met}), mean metabolism (Met_{mean}), and maximum metabolism (Met_{max}) were measured. Twenty-four texture features were compared between treated and untreated mice. Immunohistochemical mean tumor vascular density was estimated by anti-CD-34 staining after tumor resection.**

Results **Treated mice had significantly lower tumor vascular density ($P = 0.032$), confirming the antiangiogenic therapeutic effect of bevacizumab. None of the conventional measures were different between the two groups: Δ_{vol} ($P = 0.9$), Vol_{cal} ($P = 0.7$), Vol_{met} ($P = 0.28$), Met_{max} ($P = 0.7$), or Met_{mean} ($P = 0.32$). One texture parameter, GLSZM-SZV (visually indicating that the ^{18}F-FDG PET images of treated mice comprise uniformly sized clusters of different activity) had significantly different means between the two groups of mice ($P = 0.001$).**

Conclusion **^{18}F-FDG PET derived texture parameters, particularly GLSZM-SZV, may be valid biomarkers of tumor response to treatment with bevacizumab, before change in volume.** ***Nucl Med Commun*** **00:000–000**

Nuclear Medicine Communications 2019, **00**:000–000

Keywords: colorectal cancer, ^{18}F-FDG PET, texture analysis, tumor heterogeneity, xenograft

[a]Department of Radiology, Barts and London NHS Trust, [b]Department of Cancer Imaging, School of Biomedical Engineering and Imaging Sciences, [c]PET Imaging Centre and the Division of Imaging Sciences and Biomedical Engineering, King's College London and [d]Department of Radiology, Guy's Hospital, London, UK

Correspondence to Usman Bashir, FRCR, Department of Radiology, St Bartholomew's Hospital, W Smithfield, London EC1A 7BE, UK
Tel: +44 759 845 4470; fax: +44 020 8223 8852;
e-mail: drusmanbashir@gmail.com

*Usman Bashir and Amanda Weeks contributed equally to the writing of this article.

Received 11 December 2018 **Accepted** 24 January 2019

Introduction

Early detection of response to treatment is an increasingly important goal in personalized medicine. Bevacizumab is a monoclonal antibody to the vascular endothelial growth factor-A (VEGF-A) receptor [1]. It selectively targets immature new vessels within tumors and has a vascular maturation effect, whereby highly permeable, immature vessels are replaced by more mature vessels [1–3]. These changes manifest as decreasing vascular permeability in tumor regions rich in VEGF-A expression [4,5]. Because of the reported survival benefits of bevacizumab, several regimens combining bevacizumab with cytoreductive agents are being used in the treatment of colorectal cancer [1]. Like most anticancer therapeutic regimens, early response assessment is critical to identify nonresponders and switch regimens.

Because bevacizumab is not cytoreductive, responding tumors may not decrease in size early during treatment making serial size measurement on morphologic imaging unreliable for response assessment [4]. Dynamic computed tomography (CT) and MRI have shown promise in directly measuring the antiangiogenic effect of bevacizumab treatment [2,4]. However, the relatively complex nature of some of these CT and MRI protocols limits their use to institutions that have the technical expertise [6]. Furthermore, as most of these protocols utilize contrast media, patients with poor renal function cannot benefit from them. ^{18}F-FDG PET imaging has also been used to determine metabolic changes in tumors undergoing bevacizumab treatment [2,7,8]. Conventionally, metrics of tumor metabolism have been based on whole-tumor assessment, for example, mean standardized uptake value

0143-3636 DOI: 10.1097/MNM.0000000000000992

(SUV_{mean}) and metabolically active tumor volume (Vol_{met}), or measurement of single voxel-values, for example, SUV_{max}. With regard to their use as early response indicators in bevacizumab treatment, reports are conflicting. Whereas studies using bevacizumab combined with cytotoxic treatment have shown their potential as early response detectors [7–9], several authors have indicated a noncorrespondence between vascular functional and metabolic response in tumors undergoing bevacizumab monotherapy [10].

With growing interest in measuring tumor heterogeneity, investigators have discovered several ^{18}F-FDG PET-derived heterogeneity parameters as a potential alternative biomarker of response to treatment in different cancers [11–15]. These heterogeneity parameters encode additional spatial information as opposed to whole-tumor derived metrics such as SUV_{mean}, SUV_{max}, and Vol_{met}, which convey no information regarding spatial tumor heterogeneity. Because of the known tumor heterogeneity in VEGF-A expression [16], it is logical to expect differences in metabolic heterogeneity in treated tumors, with regions of high VEGF-A expression responding to bevacizumab differently from those with low VEGF-A expression.

We hypothesized that ^{18}F-FDG PET-derived parameters of spatial heterogeneity may be superior in response assessment compared with whole-tumor-based parameters such as morphologic tumor volume (Vol_{met}), maximum metabolism (Met_{max}), and mean metabolism (Met_{mean}). Hence the objective of this exploratory case–control study was to identify potential new ^{18}F-FDG PET biomarkers of early response assessment by comparing ^{18}F-FDG PET-derived texture parameters with five conventional parameters, that is, morphologic tumor volume (Vol_{cal}), change in morphologic tumor volume (Δ_{vol}), Vol_{met}, Met_{max}, and Met_{mean}, in colorectal xenograft models treated with bevacizumab.

Materials and methods

Animal studies were carried out in accordance with UK Research Council's and Medical Research Charities' guidelines on responsibility in the use of animals in bioscience research under a UK home office license. Fourteen CD1/nu/nu athymic nude mice (Charles River, Harlow, UK) were inoculated subcutaneously in the right dorsal flank with poorly differentiated colon adenocarcinoma cells (cell line LS174T; 5×10^6 cells/mouse) [17]. The tumors were allowed to grow for 3 weeks until they reached 6–9 mm diameter by caliper measurement. After 3 weeks, baseline tumor volumes (length $\times$ width^2/2 [18]) were measured with calipers. Seven mice (treatment group) were treated with bevacizumab (Avastin; Genentech, San Francisco, California, USA) at a dose of 5 mg/kg through intraperitoneal injection on alternate weekdays for six doses. The remaining seven mice were left untreated as control group. After 2 weeks of treatment, final volumes (Vol_{cal}) were calculated with calipers in all mice to document tumor growth as percent change in tumor volume: $\Delta_{vol} = 100 \times$ (final volume − baseline volume)/baseline volume.

NanoPET/CT imaging of both groups of mice was performed with a small animal Bioscan NanoPET/CT (Mediso, Budapest, Hungary). For PET scanning, all mice were anesthetized with inhalational isoflurane (induction isoflurane 4% at 0.8–1 l/min followed by isoflurane 2.5% by anesthetic mask at 0.8 l/min) throughout the scanning with respiratory monitoring and mouse bed temperature maintained at 30°C. All mice received 5 ± 0.2 MBq of ^{18}F-FDG PET by tail vein followed by PET imaging acquired at 45–60 min. Images were reconstructed with the ordered subset expectation maximization algorithm using NanoPET/CT scanner embedded software using an energy window of 400–600 keV, coincidence relation of 1–3, and isotropic voxel dimensions of 0.6 mm. After decay correction, voxel uptake values were converted to percentage injected dose per gram of tissue (% ID/g) assuming a tissue density of 1 g/cm^3. The reconstructed images were then transferred in Digital Imaging and Communications in Medicine format to MATLAB R2012b (MathWorks Inc., Natick, Massachusetts, USA) for analysis.

Texture features were analyzed in ^{18}F-FDG PET/CT images using an in-house software implemented in MATLAB (Release 2016b; The MathWorks Inc.). The tumors were delineated with the fuzzy locally adaptive Bayesian (FLAB) algorithm as follows: First, a crude bounding volume was manually drawn encompassing the entire tumor and 1–3 mm of adjacent background region [19]. This bounding volume was subjected to FLAB which classified all voxels into three classes: tumor, background, and region of partial volume averaging. The FLAB algorithm used to classify the voxels is described in detail by Hatt *et al.* [19]. A final volume of interest (VOI) was obtained by discarding voxels classified as background. The VOI was quantized into 64 equally sized bins. One hundred and fourteen computational features (15 geometric, six model-based, 37 first-order, 21 second-order, and 35 higher-order texture features) were derived from each VOI. Geometric features describe tumor morphological features such as volume, diameter, and surface-to-volume ratio. Model-based features, that is, those derived from the fractal dimension of the VOI, describe texture complexity at multiple scales. First-order texture features such as maximum and mean metabolism (i.e. highest activity voxel in the VOI), skewness, and kurtosis are based on statistical histograms and give no information on the spatial distribution of voxels within the image. Second-order features are derived from gray-level co-occurrence matrices and are locoregional, providing information on pair-wise co-occurrence of gray values in a given direction. Higher-order locoregional texture features include gray-level run length, gray-level size zone, and neighborhood gray tone difference matrices. These take larger neighborhoods of

similar gray values in different ways in three-dimension [20–22].

Following imaging, all mice were sacrificed and their tumors excised and analyzed as follows: First, pathologic tumor specimens were stained for CD34 antibodies (a marker of vascularity) using mouse monoclonal antibody to CD34 with biotinylated rat anti-mouse immunoglobulins (Vector Laboratories, Burlingame, California, USA) [23]. An enhanced biotin/avidin immunoperoxidase system, Vectastain ABC kit (Vector Laboratories) and liquid 3,3′-diaminobenzidine + chromogen (Dako, Ely, Cambridgeshire, UK) were used to detect antibody binding. Stained sections were viewed under a 10x objective on a Leica DMRB light microscope with an automated stage (Leica Microsystems Ltd, Milton Keynes, UK). Images of whole-tumor sections were captured and tiled using a QICAM FAST1394 color camera (QImaging Corporation, Burnaby, Canada) and Surveyor software (Objective Imaging Ltd, Cambridge, UK) [23]. Image analysis was performed with the operator (A.W.) blinded to mouse and treatment groups in (ImageJ; NIH, Bethesda, Maryland, USA) to determine percentage area of the tumor section with positive 3,3′-diaminobenzidine staining. Microvessel density (MVD) was determined by manually counting stained vessels in ImageJ. Stained vessels were highlighted by adjusting the color threshold (hue, saturation, and brightness) and the image was overlaid with a 1000×1000 pixel grid to aid counting.

Statistical analysis

Continuous variables were reported as mean ± SD. The Shapiro–Wilk test was used to determine which variables were normally distributed. For normally distributed variables, differences of means were compared between treated and control mice using the Welch-corrected two-sample *t*-test, whereas for non-normally distributed variables, the differences of medians were compared using the Wilcoxon signed-rank test.

Pathological response to bevacizumab treatment was confirmed by comparing mean MVD of treated versus control mice. To determine whether there was any tumor-growth delay in treated versus control mice, Δ_{vol} were compared as the difference of medians between treated and control mice. Likewise, medians of Vol_{met} and Met_{mean} determined from ^{18}F-FDG PET imaging were also compared between the treated and control mice to determine the role of conventional ^{18}F-FDG PET in differentiating the two groups.

Finally, ^{18}F-FDG PET-derived texture variables were compared between treated and untreated mice. The starting variable-set of 114 variables was reduced by excluding highly correlated variables using 'caret' package of R version 3.3.1 (The R Foundation, Vienna, Austria), using 0.8 as the cutoff for pair-wise absolute correlation [24]. The remaining variables were compared between treated and control mice for difference of means (or medians as appropriate). Bonferroni correction was applied to the *P* values to mitigate false positives arising from multiple testing using a *P* value of 0.002. Differences between the two groups were summarized in a table and illustrated by bar plots. The length of each bar would indicate fold change in a variable with respect to the control group. Fold change was computed using the formula: (value in the treated group − value in the control group)/value in control group. For example, a fold change of 0 would indicate no change, +1 would indicate that the mean value in the treatment group was twice that of control, and −1 would indicate that the mean value for the treatment group was half that of the control group.

Results

Treated tumors showed a lower number of CD34 positive vessels per unit area than control tumors, that is, 2.91×10^{-6} versus 6.57×10^{-6} ($P = 0.032$) confirming pharmacologically effective administration of bevacizumab. Measured directly with calipers, treated and control mice had mean Vol_{cal} of $312 \pm 72.93\ mm^3$ and $352 \pm 47.5\ mm^3$, respectively ($P = 0.7$). There were no significant growth delays from bevacizumab treatment of treated mice, with both groups showing similar mean Δ_{vol} of $424.53 \pm 238.7\%$ (treated) versus $434.8 \pm 117.9\%$ (control, $P = 0.9$; Fig. 1).

Conventional imaging metrics response

Standard methods of response assessment with ^{18}F-FDG PET showed no differences between treated and control mice: treated and control mice showed similar median Vol_{met} of 375 ± 96.9 versus $384.9 \pm 60.2\ mm^3$ ($P = 0.28$), Met_{max} of 43.14 ± 15.3 versus $47.6 \pm 25.7\%$ID/g ($P = 0.7$), and Met_{mean} of 14.22 ± 5.32 versus $17.85 \pm 7.5\%$ID/g ($P = 0.32$; Fig. 1).

^{18}F-FDG PET-derived texture parameter response

After excluding highly correlated texture parameters, 24 texture features remained. These were six first-order, four second-order, seven high-order statistical features, five geometric, and two model-based features (Table 1). Four variables were statistically significantly different between the two groups, that is, surface area to volume ratio ($P = 0.004$), fractal dimension maximum (FD_{max}; $P = 0.03$), gray-level run-length short-run emphasis (GLRL-SRE; $P = 0.02$), and gray-level size-zone matrix size zone variability (GLSZM-SZV; $P = 0.001$). After applying the Bonferroni-adjusted *P* value cutoff ($P < 0.002$), one variable remained (GLSZM-SZV; $P = 0.001$). Treated mice showed GLSZM-SZV that was on average −0.74-fold (or 26%) that of control mice. Figure 2 provides a graphical summary of fold change (with respect to control group) in each of the 24 texture variables.

Fig. 1

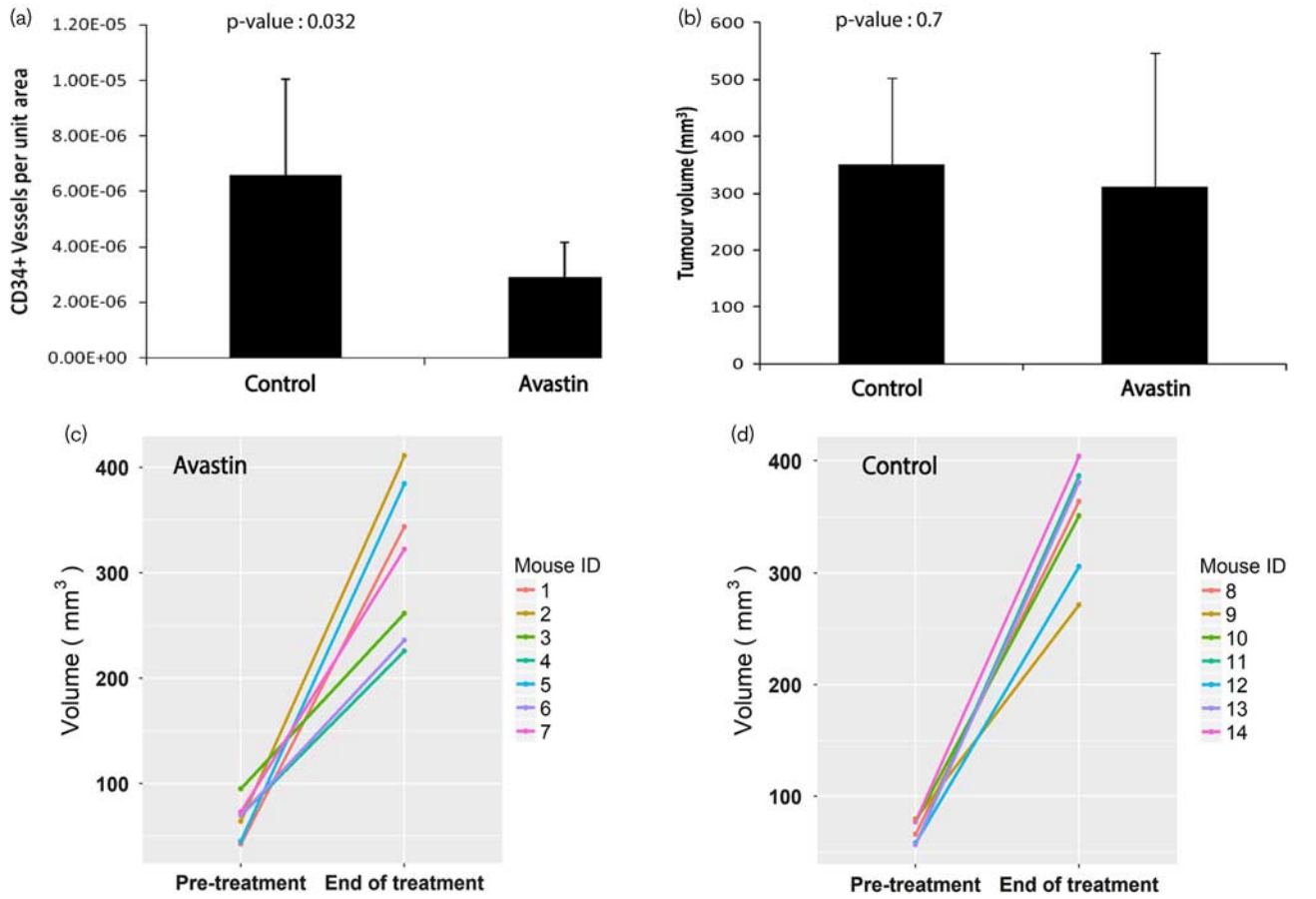

Comparing treated and control mice in terms of differences in MVD (a), volumes (caliper-measured) (b), and temporal change in volume of tumors in treated mice (c) and control mice (d). In (a) and (b), the heights of the bars denote mean values of tested variables and whiskers, the SEM. As shown in (a), there were significant differences in MVD between treated and control mice, confirming pathologic response to bevacizumab in treated mice. However, final tumor volumes of (b) and Δ_{vol} of treated and untreated mice (c and d, respectively) were not significantly different. MVD, microvessel density.

Discussion

In our study, we assessed conventional response biomarkers and a number of texture parameters in a mouse xenograft colorectal cancer model treated with antiangiogenic targeted agent bevacizumab. Our study was based on the premise that tumors treated with bevacizumab do not undergo changes in size early because of the cytostatic rather than cytoreductive effect of bevacizumab; however, we hypothesized that there may be changes within the tumor microenvironment secondary to the vascular remodeling following bevacizumab treatment that may be detectable and quantifiable by ^{18}F-FDG PET texture analysis. We found that after 2 weeks of bevacizumab treatment, four ^{18}F-FDG PET-derived texture parameters, that is, surface-to-volume ratio, FD_{max}, GLSZM-SZV, and GLRL-SRE, were significantly different between treated and control mice. After applying Bonferroni correction for multiple comparisons, a single parameter, GLSZM-SZV (−0.74-fold difference; $P=0.001$), remained significant. In contrast, conventional descriptors of tumor response, that is, morphologic tumor volumes and metabolism (Met_{max} and Met_{mean}), were not significantly different between the two groups of mice.

The GLSZM provides an estimation of a bivariate conditional probability density function of image distribution values [25]. The more homogeneous the texture, the wider and flatter the matrix. High GLSZM-SZV is an indicator of inhomogeneity; for any given gray-level intensity, there are numerous patches of different sizes. In our study, treated mice had much smaller values of GLSZM-SZV compared with control mice, which can be interpreted as their ^{18}F-FDG PET images showing little variation in sizes of isometabolic patches. Although, GLSZM-SZV by itself does not allow interpretation of the sizes of patches, the patch sizes can be inferred to be generally smaller in treated mice, based on their generally higher GLRL-SRE (0.38-fold difference; $P=0.02$) and FD_{max} (0.22-fold difference; $P=0.03$), even though

Table 1 Summary differences in mean texture parameters between treated and control mice

Texture parameters	Mean (treated)	Mean (control)	Fold change	*P* value (test used)
Geometric				
Surface area: volume (mm^{-1})*	121.85	138.17	−0.12	0.004[a]
Eccentricity	0.7	0.64	0.09	0.3[b]
Compactness	0.008	0.0078	0.02	0.81[b]
Solidity	0.837	0.832	0.01	0.46[a]
Spikiness	13.71	15.15	−0.09	0.47[b]
Model				
FD-STD	0.23	0.228	0.01	0.92[b]
FD_{max}*	4.28	3.52	0.22	0.03[b]
First-order				
First-order entropy	4.24	4.29	−0.01	0.8[a]
Coefficient of variation	0.442	0.436	0.014	0.9[b]
Kurtosis	3.85	3.09	0.24	0.38[a]
Skewness	0.66	0.6	0.1	0.79[b]
Metabolism (min) (%ID/g)	2.0	3.48	−0.42	0.24[b]
Total lesion metabolism (mm^3 %ID/g)	4.76	7.11	−0.33	0.01[b]
Second-order				
GLCM CP	6.2×10^5	4.9×10^5	0.26	0.53[b]
GLCM CS	4.9×10^3	4.5×10^3	0.09	0.87[b]
GLCM IMC	0.86	0.87	−0.007	0.85[b]
GLCM max probability	0.013	0.01	0.26	0.32[a]
Higher-order				
GLSZM size zone variability†	475.47	1822.52	−0.74	0.001[a]
GLSZM LZHIE	9.3×10^5	2.9×10^5	2.23	0.21[a]
GLSZM LIZE	0.56	0.54	0.03	0.21[b]
GLSZM zone percentage	0.16	0.17	−0.07	0.76[b]
GLRL long run HGLE	1123.89	914.58	0.23	0.34[b]
GLRL short-run HGLE	3.42	2.44	0.4	0.9[a]
GLRL-SRE*	0.07	0.05	0.38	0.02[a]

FD, fractal dimension; FD-STD, FD-standard deviation; GLCM, gray-level co-occurrence matrix; GLCM CP, GLCM cluster prominence; GLCM CS, GLCM cluster shade; GLCM IMC, GLCM information measure correlation; GLRL, gray-level run-length; GLRL long run HGLE, GLRL long run high gray-level run emphasis; GLRL-SRE, GLRL short-run emphasis; GLSZM, gray-level size-zone matrix; GLSZM LIZE, GLSZM low-intensity zone emphasis; GLSZM LZHIE, GLSZM long zone high-intensity emphasis.
[a]Wilcoxon signed-rank sum test.
[b]*t*-Test.
*$P < 0.05$ (unadjusted).
†$P < 0.002$ (Bonferroni-adjusted).

both variables were excluded after applying the Bonferroni-adjusted *P* value cutoff of 0.002. GLRLs compute contiguous sequences of voxels displaying similar gray levels in given directions. A high GLRL-SRE value indicates a finely textured image dominated by short runs of voxel gray levels [26]. Likewise, a high FD_{max} value corresponds to a high frequency of variation in voxel gray levels, that is, a fine texture [27,28]. Finally, we found a surface-to-volume ratio to be significantly lower in the treatment group (−0.12-fold difference; $P = 0.004$). This finding suggests that treated tumors became more compact and approached a spheroidal, as opposed to irregular, shape. Looking at these combinations of geometric and texture variables, it appears that ^{18}F-FDG activity in treated tumors was more compact and exhibited finer variation spatially, whereas untreated tumors were more irregular and exhibited a coarser metabolic texture.

There are only a few reports investigating the metabolic and functional effects of early bevacizumab treatment as monotherapy. These studies are generally in agreement with ours. Willett *et al.* [2] monitored six patients with rectal cancer on treatment with bevacizumab. After 12 days of bevacizumab treatment, the authors found that only one of five patients experienced tumor regression and another one patient experienced a decrease in tumor ^{18}FDG uptake, the rest showing stable tumor sizes and metabolic activity respectively. In contrast, tumor perfusion decreased by 40–45% and blood volume by 16–39% in most patients. The authors did not test spatial metabolic texture indices as response biomarkers, however. Our findings based on caliper and ^{18}F-FDG PET measurements of tumor volumes and Met_{max}, as well as Metmean, are in concordance with the results reported by Willet and colleagues. Kim *et al.* [3] measured CT-derived flow parameters and ^{18}F-FDG PET-derived SUV_{max}, SUV_{mean}, total lesion glycolysis, gray-level co-occurrence matrix (GLCM) entropy, and GLCM homogeneity in a case–control rabbit VX2 tumor model (used to model hepatocellular carcinoma) [29]. Serial imaging performed up to 14 days following treatment with bevacizumab did not show any significant differences between the two groups of rabbits in any of the ^{18}F-FDG PET-derived metrics, whereas CT-derived blood flow and blood volume were different. In our study, we also did not find significant differences in Met_{max}, Met_{mean}, or first-order entropy, although we found GLSZM-SZV to be significantly different between the two groups – not tested by Kim and colleagues. We believe that GLCM-derived features extract different textural information

Fig. 2

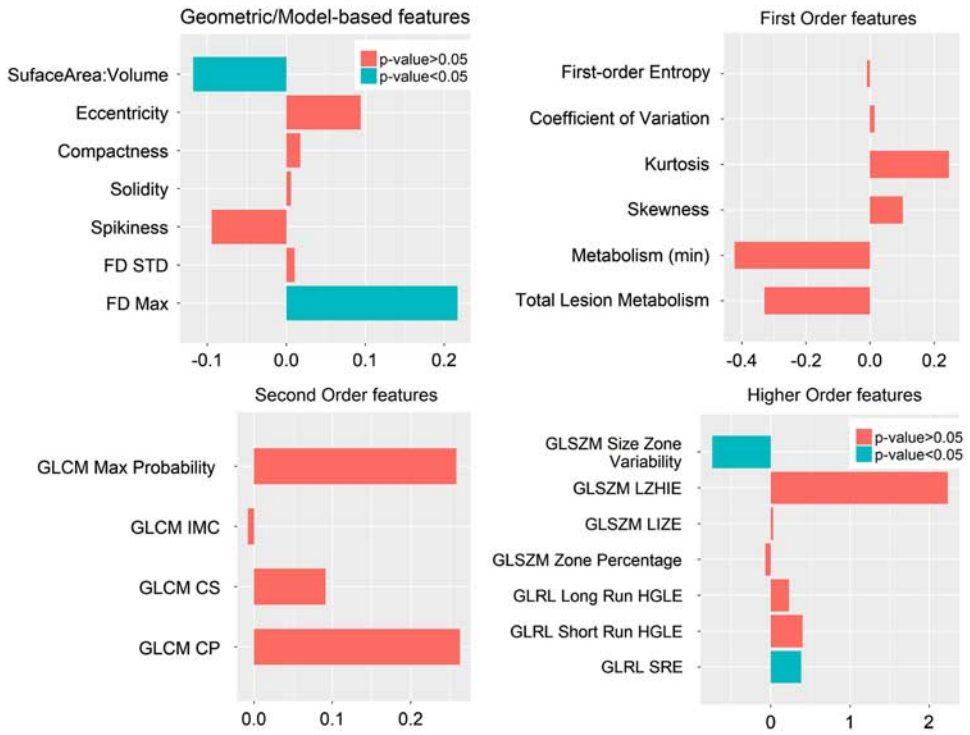

Bar plots illustrating differences in median values of individual texture parameters left after excluding highly correlated features. Four subplots are generated after grouping texture features together. Bars pointing toward the left indicate that corresponding texture features were lower in the treatment group versus the control group. Statistically, significant differences are indicated in blue. FD, fractal dimension; FD-STD, FD-standard deviation; GLCM, gray-level co-occurrence matrix; GLCM CP, GLCM cluster prominence; GLCM CS, GLCM cluster shade; GLCM IMC, GLCM information measure correlation; GLRL, gray-level run-length; GLRL long run HGLE, GLRL long run high gray-level run emphasis; GLRL-SRE, GLRL short-run emphasis; GLSZM, gray-level size zone matrix; GLSZM LIZE, GLSZM low-intensity zone emphasis; GLSZM LZHIE, GLSZM long zone high-intensity emphasis.

compared with GLSZM-derived features, as indicated by the absence of correlation between GLCM-derived and GLSZM-derived features in our study – GLCM entropy was found to be correlated with first-order entropy ($r=0.87$; $P=0.001$) and hence only first-order entropy was retained for further analysis.

A potential limitation of this study is that our sample size of 14 mice was relatively small, as is typical of xenograft studies [30], and it is possible that further texture features could have shown statistical significance with a larger cohort. Furthermore, our findings only reflect changes in tumor metabolism in response to bevacizumab, whereas, in typical clinical scenarios, bevacizumab is given in combination with chemotherapy. Nonetheless, we believe that quantification of tumor size and metabolic effects of bevacizumab monotherapy are useful to enable elucidation of its relative contribution (or lack thereof) in different scenarios of combination treatments.

Conclusion

The findings from this exploratory study suggest that early during treatment with bevacizumab, responding tumors may undergo metabolic changes in the microenvironment manifesting as a transition from coarse to fine texture of ^{18}F-FDG distribution and from an irregular to a more compact shape. In contrast, tumor sizes and maximum (or mean) metabolism do not change significantly during early bevacizumab treatment and are not reliable biomarkers of early response. These preliminary findings will need prospective evaluation in human studies, but offer novel biomarkers of treatment response to bevacizumab treatment that may be more accurate than conventional size or metabolic activity parameters.

Acknowledgements

The authors acknowledge financial support from the King's College London/University College London Comprehensive Cancer Imaging Centres funded by Cancer Research UK and Engineering and Physical Sciences Research Council in association with the Medical Research Council and the Department of Health (C1519/A16463); from the Wellcome/EPSRC Centre for Medical Engineering at King's College London (WT 203148/Z/16/Z).

Conflicts of interest

There are no conflicts of interest.

References

1 Los M, Roodhart JM, Voest EE. Target practice: lessons from phase III trials with bevacizumab and vatalanib in the treatment of advanced colorectal cancer. *Oncologist* 2007; **12**:443–450.

2 Willett CG, Boucher Y, di Tomaso E, Duda DG, Munn LL, Tong RT, *et al*. Direct evidence that the VEGF-specific antibody bevacizumab has antivascular effects in human rectal cancer. *Nat Med* 2004; **10**:145–147.

3 Kim JI, Lee H-J, Kim YJ, Kim KG, Lee KW, Lee JH, *et al*. Multiparametric monitoring of early response to antiangiogenic therapy: a sequential perfusion CT and PET/CT study in a rabbit VX2 tumor model. *ScientificWorldJournal* 2014; **2014**:701954.

4 Gaustad J-V, Simonsen TG, Smistad R, Wegner CS, Andersen LM, Rofstad EK. Early effects of low dose bevacizumab treatment assessed by magnetic resonance imaging. *BMC Cancer* 2015; **15**:900.

5 Jain RK. Normalization of tumor vasculature: an emerging concept in antiangiogenic therapy. *Science* 2005; **307**:58–62.

6 O'Connor JPB, Tofts PS, Miles KA, Parkes LM, Thompson G, Jackson A. Dynamic contrast-enhanced imaging techniques: CT and MRI. *Br J Radiol* 2011; **84**:S112–S120.

7 Vriens D, de Geus-Oei L-F, Heerschap A, van Laarhoven HW, Oyen WJ. Vascular and metabolic response to bevacizumab-containing regimens in two patients with colorectal liver metastases measured by dynamic contrast-enhanced MRI and dynamic ^{18}F-FDG-PET. *Clin Colorectal Cancer* 2011; **10**:1–5.

8 Goshen E, Davidson T, Zwas ST, Aderka D. PET/CT in the evaluation of response to treatment of liver metastases from colorectal cancer with bevacizumab and irinotecan. *Technol Cancer Res Treat* 2006; **5**:37–43.

9 Lastoria S, Piccirillo MC, Caracò C, Nasti G, Aloj L, Arrichiello C, *et al*. Early PET/CT scan is more effective than recist in predicting outcome of patients with liver metastases from colorectal cancer treated with preoperative chemotherapy plus bevacizumab. *J Nucl Med* 2013; **54**:2062–2069.

10 Miles KA, Williams RE. Warburg revisited: imaging tumour blood flow and metabolism. *Cancer Imaging* 2008; **8**:81–86.

11 Yip C, Davnall F, Kozarski R, Landau DB, Cook GJ, Ross P, *et al*. Assessment of changes in tumor heterogeneity following neoadjuvant chemotherapy in primary esophageal cancer. *Dis Esophagus* 2015; **28**:172–179.

12 Cook GJR, O'Brien ME, Siddique M, Chicklore S, Loi HY, Sharma B, *et al*. Non-small cell lung cancer treated with erlotinib: heterogeneity of ^{18}F-FDG uptake at PET-association with treatment response and prognosis. *Radiology* 2015; **276**:883–893.

13 Bashir U, Azad G, Siddique MM, Dhillon S, Patel N, Bassett P, *et al*. The effects of segmentation algorithms on the measurement of 18F-FDG PET texture parameters in non-small cell lung cancer. *EJNMMI Res* 2017; **7**:60.

14 De Cecco CN, Ganeshan B, Ciolina M, Rengo M, Meinel FG, Musio D, *et al*. Texture analysis as imaging biomarker of tumoral response to neoadjuvant chemoradiotherapy in rectal cancer patients studied with 3-T magnetic resonance. *Invest Radiol* 2015; **50**:239–245.

15 Goh V, Ganeshan B, Nathan P, Juttla JK, Vinayan A, Miles KA. Assessment of response to tyrosine kinase inhibitors in metastatic renal cell cancer: CT texture as a predictive biomarker. *Radiology* 2011; **261**:165–171.

16 Oosting SF, Brouwers AH, van Es SC, Nagengast WB, Oude Munnink TH, Lub-de Hooge MN, *et al*. ^{89}Zr-bevacizumab PET visualizes heterogeneous tracer accumulation in tumor lesions of renal cell carcinoma patients and differential effects of antiangiogenic treatment. *J Nucl Med* 2015; **56**:63–69.

17 Pedley RB, Sharma SK, Boxer GM, Boden R, Stribbling SM, Davies L, *et al*. Enhancement of antibody-directed enzyme prodrug therapy in colorectal xenografts by an antivascular agent. *Cancer Res* 1999; **59**:3998–4003.

18 Faustino-Rocha A, Oliveira PA, Pinho-Oliveira J, Teixeira-Guedes C, Soares-Maia R, da Costa RG, *et al*. Estimation of rat mammary tumor volume using caliper and ultrasonography measurements. *Lab Anim (NY)* 2013; **42**:217–224.

19 Hatt M, Cheze le Rest C, Descourt P, Dekker A, De Ruysscher D, Oellers M, *et al*. Accurate automatic delineation of heterogeneous functional volumes in positron emission tomography for oncology applications. *Int J Radiat Oncol Biol Phys* 2010; **77**:301–308.

20 Davnall F, Yip CS, Ljungqvist G, Selmi M, Ng F, Sanghera B, *et al*. Assessment of tumor heterogeneity: an emerging imaging tool for clinical practice? *Insights Imaging* 2012; **3**:573–589.

21 Chicklore S, Goh V, Siddique M, Roy A, Marsden PK, Cook GJ. Quantifying tumour heterogeneity in ^{18}F-FDG PET/CT imaging by texture analysis. *Eur J Nucl Med Mol Imaging* 2013; **40**:133–140.

22 Bashir U, Siddique MM, Mclean E, Goh V, Cook GJ. Imaging heterogeneity in lung cancer: techniques, applications, and challenges. *AJR Am J Roentgenol* 2016; **207**:534–543.

23 Pusztaszeri MP, Seelentag W, Bosman FT. Immunohistochemical expression of endothelial markers CD31, CD34, von Willebrand Factor, and Fli-1 in normal human tissues. *J Histochem Cytochem* 2006; **54**:385–395.

24 Kuhn M. A short introduction to the caret package. R Proj Website; 2015. Available at: *http://202.112.154.58/cran/web/packages/caret/vignettes/caret.pdf*. [Accessed August 2016].

25 Thibault G, Angulo J, Meyer F. Advanced statistical matrices for texture characterization: application to cell classification. *IEEE Trans Biomed Eng* 2014; **61**:630–637.

26 Run Lengths (Biomedical Image Analysis). Available at: *http://what-when-how.com/biomedical-image-analysis/run-lengths-biomedical-image-analysis/*. [Accessed 4 April 2017].

27 Smith TG Jr, Lange GD, Marks WB. Fractal methods and results in cellular morphology: dimensions, lacunarity and multifractals. *J Neurosci Methods* 1996; **69**:123–136.

28 Moradi M, Mousavi P, Abolmaesumi P. Tissue characterization using fractal dimension of high frequency ultrasound RF time series. *Med Image Comput Comput Interv* 2007; **10**:900–908.

29 Bimonte S, Leongito M, Piccirillo M, de Angelis C, Pivonello C, Granata V, *et al*. Radio-frequency ablation-based studies on VX2rabbit models for HCC treatment. *Infect Agent Cancer* 2016; **11**:38.

30 Vesterinen HM, Sena ES, Egan KJ, Hirst TC, Churolov L, Currie GL, *et al*. Meta-analysis of data from animal studies: a practical guide. *J Neurosci Methods* 2014; **221**:92–102.